EUROPEAN ORGANISATION FOR NUCLEAR RESEARCH

LC-PHSM-2004-008

CLIC PHYSICS STUDY GROUP

Production of the neutral A and H Higgs bosons in e^+e^- collisions at CLIC

A. Ferrari
Department of Radiation Sciences, Uppsala University (Sweden)

Abstract

In this paper, we consider the production of A and H neutral Higgs bosons in e^+e^- collisions at 3 TeV. High energy beam-beam effects are taken into account. With an integrated luminosity of 3000 fb^{-1}, AH pairs are likely to be discovered at CLIC if m_A remains smaller than 1.2 TeV at small $tan\beta$ (i.e. $t\bar{t}t\bar{t}$ final states) and 1.4 TeV at large $tan\beta$ (i.e. $b\bar{b}b\bar{b}$ final states). The mass and the signal rate can be measured with a χ^2-analysis. The statistical error on m_A was found to be less than 2-3%. Furthermore, the comparison of the signal rates for $b\bar{b}b\bar{b}$ and $t\bar{t}t\bar{t}$ final states allows determination of $tan\beta$ with an accuracy better than 10% in the region $4 \leq tan\beta \leq 10$.

Geneva, Switzerland
April 16, 2004

1 Introduction

One of the most important tasks of a future multi-TeV e^+e^- linear collider will be the exploration of the Higgs sector, in the Standard Model and also beyond it. The theoretical framework of the study presented in this paper is the minimal supersymmetric extension of the Standard Model (MSSM), where two complex scalar Higgs doublets are responsible for the electroweak symmetry breaking. The Higgs spectrum thus consists of five physical states. Two of them are charged (H^+ and H^-) and, among the three neutral Higgs bosons, two are CP-even states, h^0 and H, and one is CP-odd, A. The pair production of charged Higgs bosons at the Compact Linear Collider CLIC [1] was studied in a previous paper [2]. In particular, it was shown that, with an integrated luminosity of 3000 fb^{-1}, the charged Higgs bosons can be discovered at CLIC up to a mass of 1.2 TeV and that an accurate measurement of $m_{H^\pm}$ and of the signal rate can subsequently be performed. In this paper, we focus on the pair production of the heavy neutral Higgs bosons of the MSSM, by studying $e^+e^- \to AH$ at CLIC. Some detailed studies [3, 4] have already shown that this process can indeed be observed at a linear collider operating at a centre-of-mass energy of 500 or 800 GeV.

In Section 2, the cross section for $e^+e^- \to AH$ is computed at $\sqrt{s} = 3$ TeV, i.e. the nominal centre-of-mass energy at CLIC, and the various branching ratios of A and H are estimated, as a function of the MSSM parameter $tan\beta$. In Section 3, we focus on the reconstruction of the neutral Higgs bosons, taking into account the background from $\gamma\gamma \to$ hadrons. In Section 4, the discovery potential for the neutral A and H Higgs bosons at CLIC is discussed. In Section 5, we estimate the accuracy with which m_A and the signal rates for $e^+e^- \to AH$ can be measured and, in Section 6, we discuss the derivation of $tan\beta$ from these measurements. Finally, some conclusions are given in Section 7.

2 Production cross section and branching ratios of the neutral A and H Higgs bosons

2.1 Cross section for the pair production of neutral Higgs bosons at CLIC

In high-energy e^+e^- collisions, neutral Higgs bosons are produced in pairs via an intermediate photon or Z boson. At tree level, the production cross section for $e^+e^- \to H, h^0 + A$ can be computed using the Feynman rules for the coupling between Z and the neutral Higgs bosons and one obtains [5]:

$$\sigma = \frac{e^2}{48\pi} \times \left(\frac{8sin^4\theta_W - 4sin^2\theta_W + 1}{sin^2\theta_W cos^2\theta_W}\right) \times f^2 \times \frac{\kappa^3}{\sqrt{s}\,[(s-m_Z^2)^2 + \Gamma_Z^2 m_Z^2]}.$$

In this equation, the parameter f is defined as follows:

$$f = \frac{e}{2sin\theta_W cos\theta_W} \times \begin{cases} sin(\alpha - \beta) \text{ for } H \\ cos(\alpha - \beta) \text{ for } h^0 \end{cases},$$

where α is the mixing angle in the neutral CP-even sector, which is related to $tan\beta$, m_A and m_Z by:

$$tan2\alpha = tan2\beta \times \left(\frac{m_H^2 + m_{h^0}^2}{m_A^2 - m_Z^2} \right), \quad -\frac{\pi}{2} < \alpha < 0.$$

In the following, we consider a scenario where m_{h^0} is close to 115 GeV and where A and H are much heavier than h^0. This leads to $\alpha \simeq \beta - \pi/2$ and therefore to $cos(\alpha - \beta) \simeq 0$. This means that $e^+e^- \rightarrow h^0 A$ is strongly suppressed and that only AH pairs can be produced. Furthermore, when $m_A \gg m_Z$, the mass difference between H and A is a few GeV at small $tan\beta$ and only a fraction of GeV at large $tan\beta$: A and H are thus almost degenerate in mass.

As for the parameter κ, it is given by:

$$\kappa = \frac{\lambda^{1/2}(s, m_H^2, m_A^2)}{2\sqrt{s}}, \text{ where } \lambda(a,b,c) = (a+b+c)^2 - 4ab.$$

The tree level production cross section for $e^+e^- \rightarrow AH$ thus reduces to:

$$\sigma = \frac{e^4}{48\pi s} \times \left(1 - 4\frac{m_A^2}{s}\right)^{3/2} \times \left(\frac{8sin^4\theta_W - 4sin^2\theta_W + 1}{32sin^4\theta_W cos^4\theta_W}\right) \times \frac{1}{(1 - m_Z^2/s)^2}.$$

Under this form, the cross section for $e^+e^- \rightarrow AH$ only depends on m_A and on the centre-of-mass energy $\sqrt{s}$.

At CLIC, in addition to the initial state radiation of photons (ISR), one must take into account high energy beam-beam effects. Because of the very small transverse dimensions of the beams at the interaction point, electrons and positrons experience very strong transverse electromagnetic fields. The bending of their trajectories induces emission of photons (beamstrahlung). In a strong external field, a photon can turn into an e^+e^- pair, and the number of additional particles due to this coherent pair creation is not negligible, even compared to the number of beam particles (4×10^9 per bunch), so they also contribute to the beam fields. In the following, the nominal centre-of-mass energy is 3 TeV and the luminosity is 10^{35} cm^{-2}.s^{-1}. The average energy loss of a beam particle due to beamstrahlung is then 31%, and the number of coherent pairs per bunch crossing is 6.6×10^8 [6]. Figure 1 shows the resulting luminosity spectrum calculated with GUINEA-PIG [7] and then implemented into the event generator.

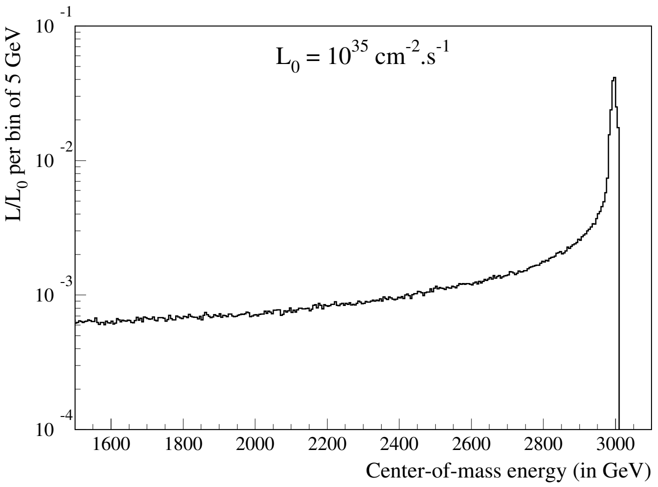

Figure 1: Luminosity spectrum at CLIC for a centre-of-mass energy of 3 TeV.

The cross section for $e^+e^- \to AH$ was computed with PYTHIA 6.1 [8]. The process 300 was used, and all s-particles were assumed to be heavier than the neutral Higgs bosons, so only the standard decays of A and H were considered. Figure 2 shows the cross section computed for a fixed centre-of-mass energy of 3 TeV and after having included ISR and beamstrahlung effects.

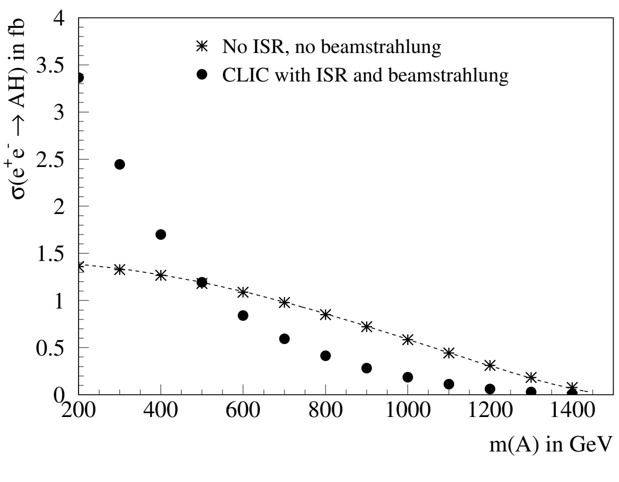

Figure 2: Cross section for $e^+e^- \to AH$: the open crosses and the dashed line show the cross section calculated at tree level, while the full circles show the cross section obtained after taking ISR and beamstrahlung effects into account.

If one considers a fixed centre-of-mass energy of 3 TeV, the calculation with PYTHIA agrees very well with the theoretical prediction at tree level (open crosses versus dashed line). When ISR and beamstrahlung effects are taken into account, one has to make a convolution of the tree level cross section with the luminosity spectrum. For the low values of m_A, since one integrates over almost the whole energy spectrum (from 1.5 TeV down to m_A), the effective cross section becomes larger than the tree level cross section. On the other hand, if m_A is close to the threshold, only a small fraction of the energy spectrum is available, so the effective cross section is smaller than the tree level cross section.

2.2 Branching ratios of the neutral *A* and *H* Higgs bosons

In the MSSM, the heavy CP-even Higgs boson H has the same decay channels as the light Higgs boson h^0 in the Standard Model and, in addition, decay cascades into two light Higgs bosons or into a mixed pair of Higgs and gauge bosons can also occur. For the CP-odd Higgs boson A, there are less decay channels because the CP-invariance forbids the pseudoscalar A to couple to gauge and Higgs boson pairs. A complete study of the decay modes of A and H is presented in [9]. In the following, we will assume that A and H do not decay into supersymmetric particles and that their mass is above the threshold for $t\bar{t}$ production. In this case, the major decay modes are those with a pair of third generation fermions, i.e. A and H both mostly decay into $t\bar{t}$, $b\bar{b}$ or $\tau\bar{\tau}$.

Several values of $tan\beta$ were considered in the 1-30 range. For each of them, the branching ratios Br$(A, H \to t\bar{t})$, Br$(A, H \to b\bar{b})$ and Br$(A, H \to \tau\bar{\tau})$ were estimated with HDECAY [10], a program which calculates the partial widths of the MSSM Higgs bosons, taking into account the running quark masses at the scale of the Higgs bosons mass. Our results are shown in Figure 3 for $m_A = 876$ GeV (other values of m_A above the $t\bar{t}$ threshold lead to very similar values of the branching ratios). For the low values of $tan\beta$, the main decay is $A, H \to t\bar{t}$ while, for the large values of $tan\beta$, there are two dominant decay modes: $A, H \to b\bar{b}$ (with a branching ratio of about 87%) and $A, H \to \tau\bar{\tau}$ (with a branching ratio of about 12%).

In the following, we only focus on the decay cascades that lead to four quarks of the third generation and we forget the $A, H \to \tau\bar{\tau}$ decays. Depending on whether the A and H Higgs bosons decay into $t\bar{t}$ or $b\bar{b}$, there are three possible final states, $t\bar{t}t\bar{t}$, $t\bar{t}b\bar{b}$ or $b\bar{b}b\bar{b}$. Figure 4 show their repartition as a function of $tan\beta$, for $m_A = 876$ GeV. Again, any other value of m_A above the $t\bar{t}$ threshold would lead to similar results. The $t\bar{t}t\bar{t}$ final states dominate at low $tan\beta$ values, while the $b\bar{b}b\bar{b}$ final states dominate at large $tan\beta$ values. For the intermediate values of $tan\beta$, the situation is more complex, since the three final states are almost equally accessible.

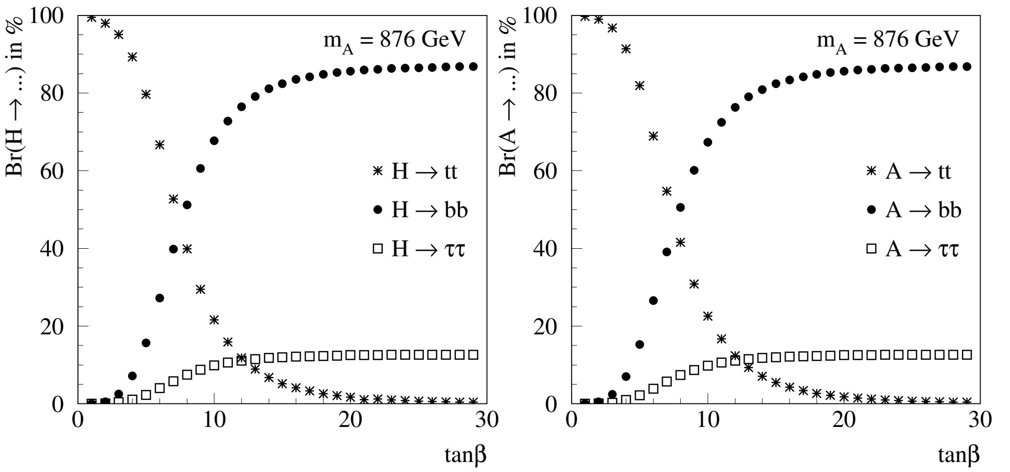

Figure 3: Branching ratios of the decays into $t\bar{t}$, $b\bar{b}$ and $\tau\bar{\tau}$ for the CP-even Higgs boson H (left) and for the CP-odd Higgs boson A (right) in the MSSM, as a function of $tan\beta$. These calculations were performed assuming that m_A is 876 GeV, i.e. above the $t\bar{t}$ threshold.

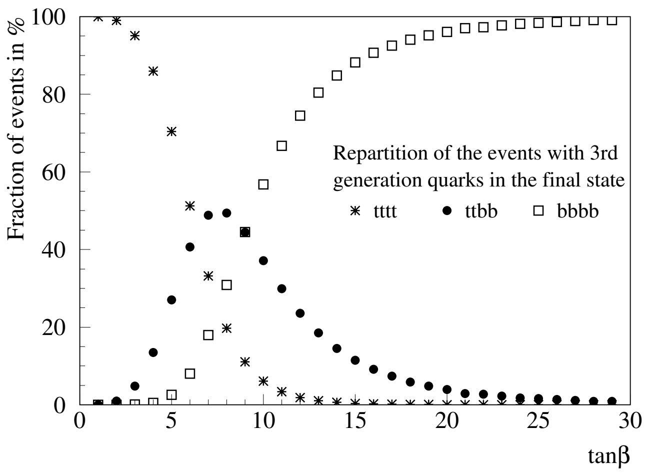

Figure 4: Repartition of the $t\bar{t}t\bar{t}$, $t\bar{t}b\bar{b}$ and $b\bar{b}b\bar{b}$ final states, as a function of $tan\beta$, after the production of AH pairs in e^+e^- collisions and after the decay of A and H into either $t\bar{t}$ or $b\bar{b}$. These calculations were performed with $m_A = 876$ GeV.

3 Reconstruction of the neutral Higgs bosons

3.1 Simulation of the detector response

Following the generation of $e^+e^- \rightarrow AH$ events, a fast detector simulation is performed by using the SIMDET code [11] with its default parametrizations for CLIC. This program applies a gaussian smearing to the momenta of the charged particles and to the energy measured in the electromagnetic and hadronic calorimeters. It takes into account the tracking efficiencies, the charge misidentification and the threshold energies for detection.

At CLIC, high energy $\gamma\gamma$ collisions will lead to the production of additional hadrons. If the nominal centre-of-mass energy is 3 TeV, one expects about 4 of these hadronic events per bunch crossing, with a centre-of-mass energy $\sqrt{s_{\gamma\gamma}}$ larger than 5 GeV [6]. The hadrons produced in the $\gamma\gamma$ collisions have a rather small transverse energy: most of them remain very close to the beam axis and, when they are found in the central part of the detector, their energy is very low. This is illustrated in Figure 5. At CLIC, bunch crossings will occur every 0.67 ns, which is much smaller than the time response of any existing or foreseen detector. One should thus integrate the contribution of the hadronic background over N_{bc} bunch crossings. About 8000 $\gamma\gamma \rightarrow$ hadrons events are stored in a database and can be added to the $e^+e^- \rightarrow AH$ events generated with PYTHIA.

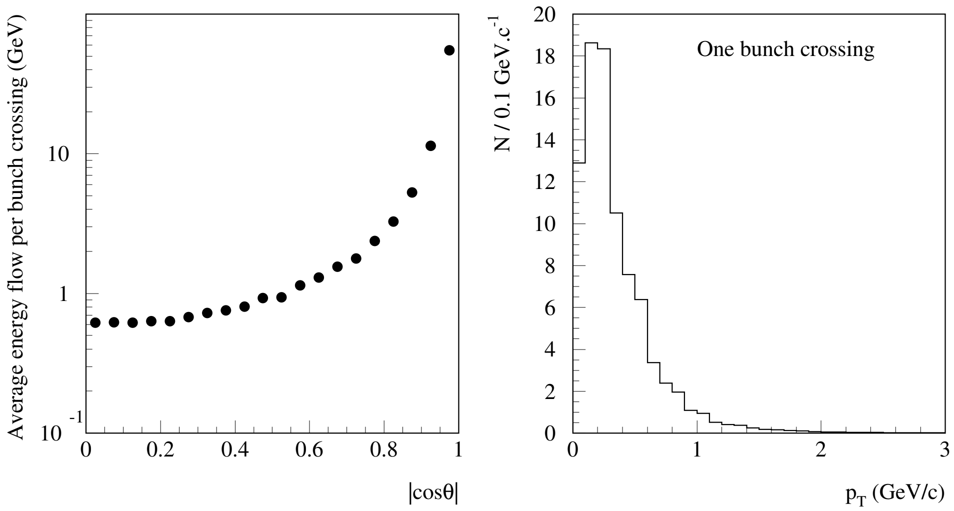

Figure 5: Average energy flow due to the hadronic background from $\gamma\gamma$ collisions per bunch crossing as a function of the angle with respect to the beam axis (left) and p_T distribution of the hadrons produced in the $\gamma\gamma$ collisions (right).

In the following, we focus on the decay cascades of A and H which produce quarks of the third generation, i.e. $e^+e^- \to AH \to b\bar{b}b\bar{b}, t\bar{t}t\bar{t}, t\bar{t}b\bar{b}$. These three processes lead to highly distinctive, yet challenging, multi-jet final states with four b tagged jets. In SIMDET, a cluster analysis method based on particle momenta is used in order to reconstruct the jets. Their multiplicity strongly depends on the distance scale d_{join} above which two clusters may not be joined in the PYCLUS subroutine of PYTHIA. The optimal value for d_{join} is obtained by maximizing the fraction of events with exactly the expected number of reconstructed jets in the final state, when no hadronic background from $\gamma\gamma$ collisions is included. As for the b tagging efficiency, it is set to 90% (if not otherwise specified) and it is then implemented by hand in the reconstruction procedure.

3.2 Reconstruction of $e^+e^- \to AH \to b\bar{b}b\bar{b}$

At large $tan\beta$, both A and H mainly decay into a $b\bar{b}$ pair. The final states to consider therefore consist of at least four hadronic jets. In addition, four of these jets must be tagged as b jets. Note that the jet multiplicity is generally larger than four, because of the additional hadronic activity which is induced by the $\gamma\gamma$ collisions (in the following, we choose $N_{bc} = 15$). However, in our analysis, none of the parasitic non-b tagged jets is used in the reconstruction of the AH pair.

There are three ways to combine the four selected b tagged jets into two (bb) systems. In each case, the mass difference $\delta m = |m(bb)_1 - m(bb)_2|$ is calculated and the combination with the smallest δm is kept, since m_A and m_H are almost degenerate (the mass splitting between A and H is indeed much smaller than the experimental mass resolution). The invariant masses of the two selected (bb) systems can be either plotted separately or binned into one single histogram, as shown in Figure 6. In the latter case, the events for which δm is larger than 250 GeV are discarded. After having assigned the b tagged jets to their correct AH pair, one can further improve the reconstruction of the neutral Higgs bosons by using a kinematical fit with the following constraints:

- the A and H candidates have the same mass,
- the system consisting of the four b tagged jets has p_x and p_y equal to zero,
- the momentum and energy conservation at $\sqrt{s} = 3$ TeV (with neither ISR nor beamstrahlung losses) is applied to an imaginary system consisting of the four b tagged jets and a neutrino with a zero transverse momentum.

After having used the kinematical fit, the mass resolution becomes almost twice better, as shown in Figure 7. For $m_A = 876$ GeV, the total signal efficiency is about 30%, after the b tagging and after the selection of the events under the peak for which the mass difference between the two (bb) systems is smaller than 250 GeV and for which the kinematical fit has converged.

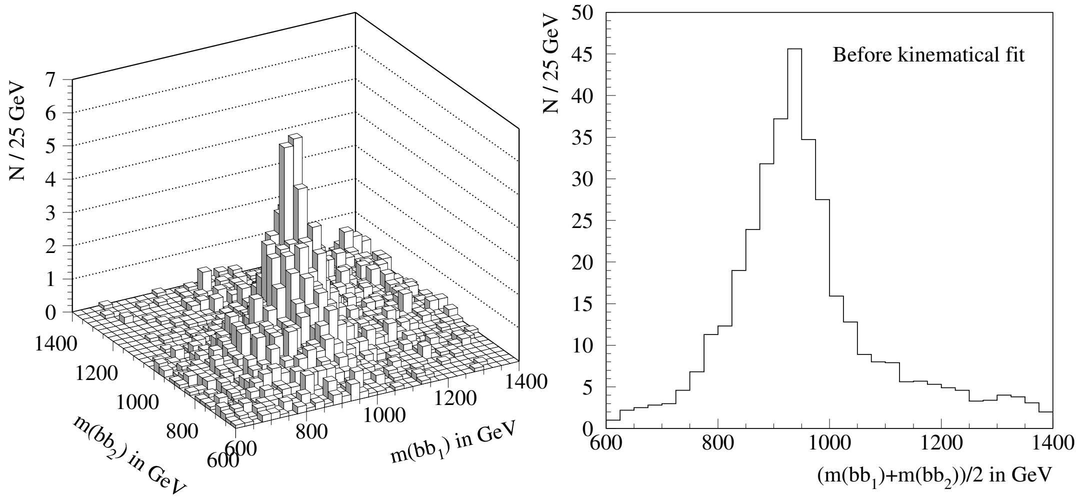

Figure 6: Mass reconstruction of a AH pair from four b tagged jets, before the kinematical fit. Here, m_A is 876 GeV, $\mathrm{Br}(A \to b\bar{b}) = \mathrm{Br}(H \to b\bar{b}) \simeq 87\%$, the plots have been normalized to an integrated luminosity of 3000 fb^{-1} and the hadronic background is taken into account, with $N_{bc} = 15$.

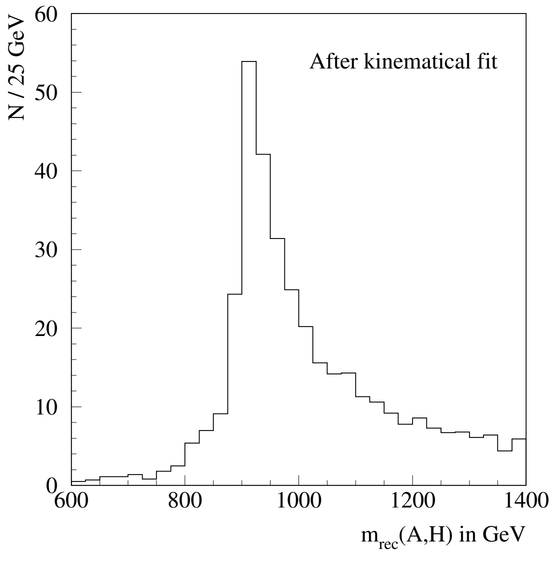

Figure 7: Mass reconstruction of a AH pair from four b tagged jets, after the kinematical fit. Here, m_A is 876 GeV, $\mathrm{Br}(A \to b\bar{b}) = \mathrm{Br}(H \to b\bar{b}) \simeq 87\%$, the plots have been normalized to an integrated luminosity of 3000 fb^{-1} and the hadronic background is taken into account, with $N_{bc} = 15$.

3.3 Reconstruction of $e^+e^- \to AH \to t\bar{t}t\bar{t}$

If $tan\beta$ is small, both A and H mainly decay into a $t\bar{t}$ pair. The final states to consider therefore consist of four b quarks and four W bosons. Here, we only focus on the hadronic decays of the W bosons and we thus search for final states with at least twelve hadronic jets, four of them being tagged as b jets.

In a first step, the presence of four W bosons decaying hadronically is tested. If there was no hadronic background, the assignment of two non-b tagged jets j_a and j_b to their correct W boson would be done by choosing the combination which minimizes $|m(j_a j_b) - m_W|$. However, since the high energy $\gamma\gamma$ collisions produce additional hadrons, which are merged into the jets, the reconstructed masses of the intermediate states are slightly higher than what they would be without the hadronic background. In order to keep a good efficiency for the jet assignment, one should replace m_W by $m_{rec}(W)$, i.e. the experimental mass peak value of the W candidates. In a second step, each t quark is reconstructed from one W candidate paired with one of the four b tagged jets, such that the invariant masses of the four (Wb) systems are as close as possible to $m_{rec}(t)$. At this stage, the events for which the jet combinations are not compatible with a W boson and a t quark, within the observed resolution, are discarded.

There are three ways to combine the four t candidates into two (tt) systems. In each case, the mass difference $\delta m = |m(tt)_1 - m(tt)_2|$ is calculated, and the combination with the smallest δm is kept (A and H are almost degenerate in mass). The invariant masses of the two selected (tt) systems can be either plotted separately or binned into one single histogram, see Figure 8. In the latter case, the events for which δm is larger than 250 GeV are discarded. After having assigned the t candidates to their correct AH pair, one can improve the reconstruction procedure by using a kinematical fit with the following constraints:

- the mass of the intermediate states are equal to m_W or m_t,
- the A and H candidates have the same mass,
- the system consisting of the four b tagged jets and the eight non-b tagged jets used to reconstruct the four t candidates has p_x and p_y equal to zero,
- the momentum and energy conservation at $\sqrt{s} = 3$ TeV (with neither ISR nor beamstrahlung losses) is applied to an imaginary system consisting of the twelve selected jets and a neutrino with a zero transverse momentum.

After having used the kinematical fit, the mass resolution is improved by nearly 30%, see Figure 9. For $m_A = 576$ GeV, the total signal efficiency is about 2%, after the b tagging and after the selection of the events under the peak for which the mass difference between the two (tt) systems is smaller than 250 GeV and for which the kinematical fit has converged.

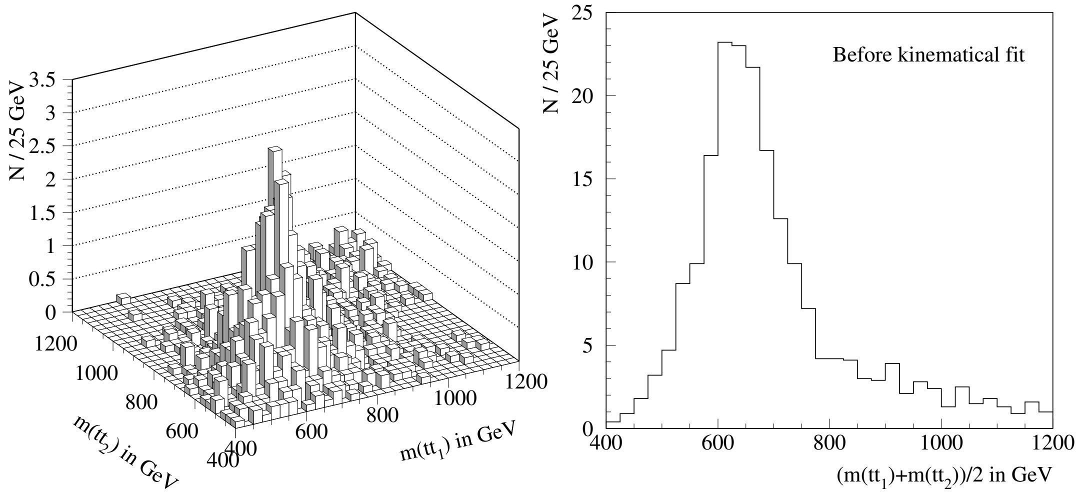

Figure 8: Mass reconstruction of a AH pair from four t candidates, before the kinematical fit. Here, m_A is 576 GeV, $\mathrm{Br}(A \to t\bar{t}) = \mathrm{Br}(H \to t\bar{t}) = 100\%$, the plots have been normalized to an integrated luminosity of 3000 fb^{-1} and the hadronic background is taken into account, with $N_{bc} = 15$.

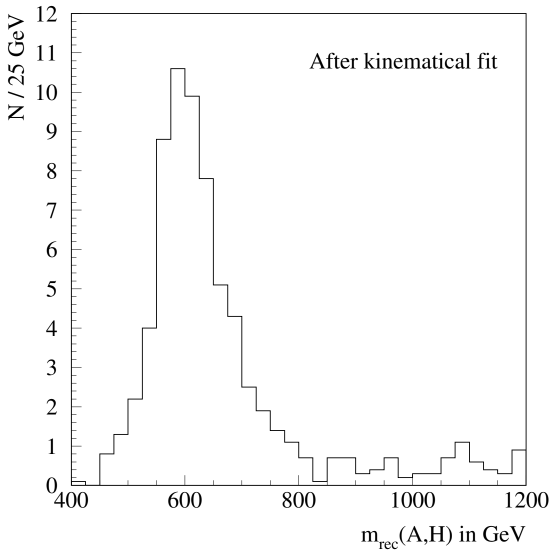

Figure 9: Mass reconstruction of a AH pair from four t candidates, after the kinematical fit. Here, m_A is 576 GeV, $\mathrm{Br}(A \to t\bar{t}) = \mathrm{Br}(H \to t\bar{t}) = 100\%$, the plots have been normalized to an integrated luminosity of 3000 fb^{-1} and the hadronic background is taken into account, with $N_{bc} = 15$.

3.4 Reconstruction of $e^+e^- \to AH \to t\bar{t}b\bar{b}$

For the intermediate values of $tan\beta$, typically in the 5-10 region, A and H can decay into $b\bar{b}$ and $t\bar{t}$ pairs, with similar branching ratios. In this configuration, a significant fraction of the $e^+e^- \to AH$ events may lead to $t\bar{t}b\bar{b}$ final states, and subsequently to four b quarks and two W bosons. In the following, we choose $tan\beta \simeq 7$ so that $\mathrm{Br}(A, H \to b\bar{b}) = \mathrm{Br}(A, H \to t\bar{t}) \simeq 46.5\%$. Furthermore, we only focus on the hadronic decays of the W bosons and we thus search for final states with at least eight hadronic jets, four of them being tagged as b jets.

In a first step, the presence of two W bosons decaying hadronically is tested. The assignment of two non-b tagged jets j_a and j_b to their correct W boson is done by choosing the combination which minimizes $|m(j_a j_b) - m_{rec}(W)|$, where $m_{rec}(W)$ is the expected mass peak value of the W candidates when taking into account the background from $\gamma\gamma \to$ hadrons. In a second step, each t quark is reconstructed from a W candidate paired with one of the four b tagged jets, such that the invariant mass of the (Wb) system is as close as possible to $m_{rec}(t)$. At this stage, the events for which the jet combinations are not compatible with a W boson and a t quark, within the observed resolution, are discarded.

Then, in order to reconstruct the neutral Higgs bosons, one pairs the two t candidates on the one hand and the two remaining b tagged jets on the other hand. The invariant masses of these two systems are shown in Figure 10. After having assigned the jets to their W and t candidates, one can further improve the reconstruction of A and H by using a kinematical fit with the following constraints:

- the mass of the intermediate states are equal to m_W or m_t,
- the A and H candidates have the same mass,
- the system consisting of the four b tagged jets and the four non-b tagged jets has p_x and p_y equal to zero,
- the momentum and energy conservation at $\sqrt{s} = 3$ TeV (with neither ISR nor beamstrahlung losses) is applied to an imaginary system consisting of the four b tagged jets, the four non-b tagged jets and a neutrino with a zero transverse momentum.

After having used the kinematical fit, the mass resolution is improved by nearly 40%, as shown in Figure 11. For $m_A = 736$ GeV, the total signal efficiency is about 4%, after the b tagging and after the selection of the events under the peak for which the kinematical fit has converged. Note that, at this stage, no cut has been applied on the mass difference between the (tt) and (bb) systems.

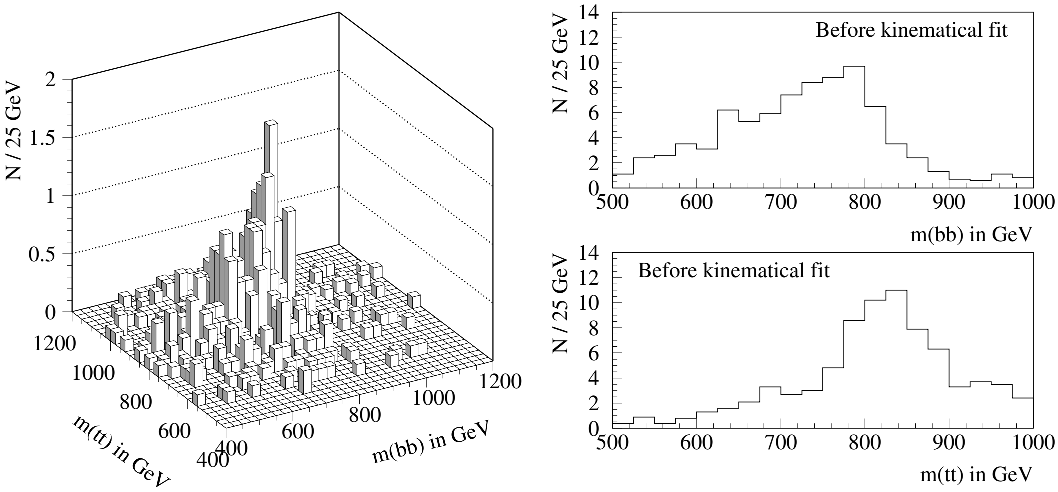

Figure 10: Mass reconstruction of a AH pair from $t\bar{t}b\bar{b}$ final states, before the kinematical fit. Here, m_A is 736 GeV, $\mathrm{Br}(A, H \to t\bar{t}) = \mathrm{Br}(A, H \to b\bar{b}) \simeq 46.5\%$, the plots have been normalized to an integrated luminosity of 3000 fb^{-1} and the hadronic background is taken into account, with $N_{bc} = 15$.

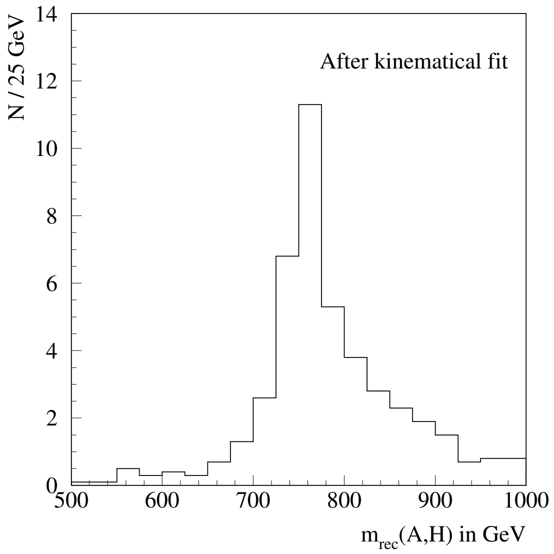

Figure 11: Mass reconstruction of a AH pair from $t\bar{t}b\bar{b}$ final states, after the kinematical fit. Here, m_A is 736 GeV, $\mathrm{Br}(A, H \to t\bar{t}) = \mathrm{Br}(A, H \to b\bar{b}) \simeq 46.5\%$, the plots have been normalized to an integrated luminosity of 3000 fb^{-1} and the hadronic background is taken into account, with $N_{bc} = 15$.

The production of H^+H^- pairs also leads to final states with four b quarks and two W bosons [2]. Since the cross section for $e^+e^- \to H^+H^-$ is 2 to 3 times larger than for $e^+e^- \to AH$ and since $H^\pm \to tb$ is the dominant decay mode of the charged Higgs boson, the signal rate for $e^+e^- \to H^+H^- \to t\bar{b}\bar{t}b$ is significantly larger than for $e^+e^- \to AH \to t\bar{t}b\bar{b}$. But the event configurations are different.

- In the case of $e^+e^- \to AH \to t\bar{t}b\bar{b}$, one (tt) system and one (bb) system are reconstructed. In general, their invariant masses are somewhat larger than the generated mass m_A, because some of the hadrons produced in the additional $\gamma\gamma$ collisions are merged into the jets originating from the decay cascades of A and H. Six jets are used to reconstruct a (tt) system, while a (bb) system consists of only two jets. This leads to a non-zero average value for the mass difference $\delta m_{tt,bb} = m_{rec}(tt) - m_{rec}(bb)$, with a standard deviation of 175 GeV, for $m_A = 736$ GeV, see the left-hand side plot of Figure 12.
- In the case of $e^+e^- \to H^+H^- \to t\bar{b}\bar{t}b$, two (tb) systems are reconstructed. The assigment of the t candidates and the b jets to their correct H^+H^- pair is done such that the mass difference $\delta m_{tb,tb} = m_{rec}(tb_1) - m_{rec}(tb_2)$ is as small as possible. Indeed, it has an average value which is close to zero, with a standard deviation of 145 GeV, for $m_A = 736$ GeV, see the right-hand side plot of Figure 12.

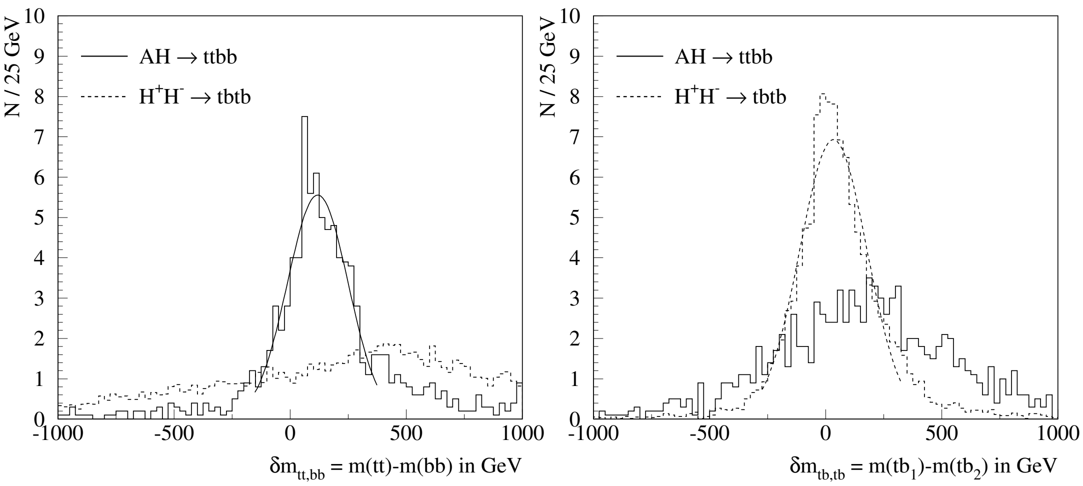

Figure 12: Comparison of $\delta m_{tt,bb}$ (left) and $\delta m_{tb,tb}$ (right) for $e^+e^- \to AH \to t\bar{t}b\bar{b}$ and $e^+e^- \to H^+H^- \to t\bar{b}\bar{t}b$, with $m_A = 736$ GeV. The hadronic background is taken into account, with $N_{bc} = 15$. For the sake of simplicity, the same number of events was used for $e^+e^- \to AH \to t\bar{t}b\bar{b}$ and $e^+e^- \to H^+H^- \to t\bar{b}\bar{t}b$.

Figure 13 shows a comparison between the mass spectrum of the (tt) and (bb) systems for $e^+e^- \rightarrow H^+H^- \rightarrow t\bar{b}\bar{t}b$ and for $e^+e^- \rightarrow AH \rightarrow t\bar{t}b\bar{b}$, after assignment of the hadronic jets to the W and t candidates and after selection of the events for which $|m_{rec}(tb_1) - m_{rec}(tb_2)| \geq 250$ GeV and $|m_{rec}(tt) - m_{rec}(bb) - \delta\tilde{m}| \leq 250$ GeV, where $\delta\tilde{m}$ is the average value of $\delta m_{tt,bb}$. For $m_A = 736$ GeV and $tan\beta \simeq 7$, there are 2 to 3 times more $AH \rightarrow t\bar{t}b\bar{b}$ events than $H^+H^- \rightarrow t\bar{b}\bar{t}b$ events under the reconstructed mass peaks.

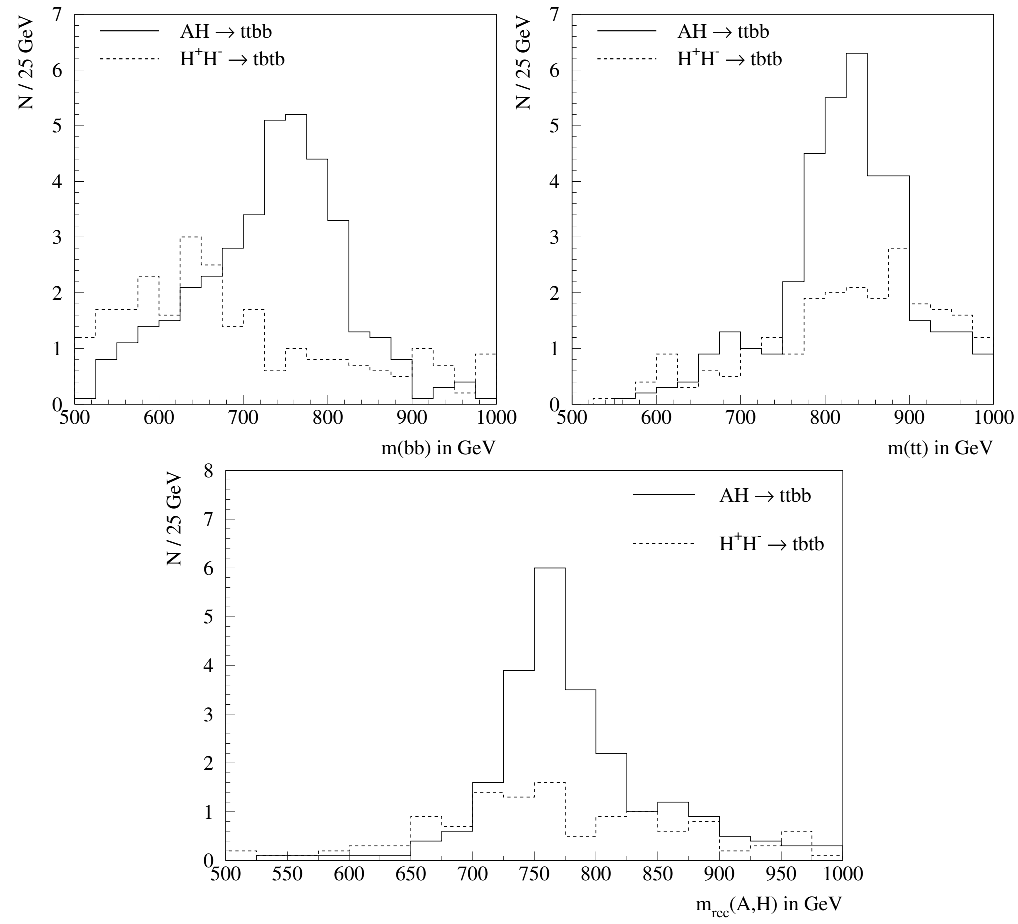

Figure 13: Comparison of the mass spectrum of the reconstructed (tt) and (bb) systems for $e^+e^- \rightarrow AH \rightarrow t\bar{t}b\bar{b}$ and for $e^+e^- \rightarrow H^+H^- \rightarrow t\bar{b}\bar{t}b$. Here, m_A is 736 GeV, $\mathrm{Br}(A, H \rightarrow t\bar{t}) = \mathrm{Br}(A, H \rightarrow b\bar{b}) \simeq 46.5\%$ and $\mathrm{Br}(H^{\pm} \rightarrow tb) = 93\%$. The plots have been normalized to an integrated luminosity of 3000 fb^{-1} and the hadronic background is taken into account, with $N_{bc} = 15$. The upper plots are obtained without the kinematical fit, while the plot at the bottom is reconstructed after having used the kinematical fit.

For the sake of simplicity, we will not consider the $e^+e^- \to H^+H^- \to t\bar{b}\bar{t}b$ events in the following, but the cuts used to reduce their contribution to a reasonably low level will be applied. In particular, when estimating the discovery potential for AH pairs at CLIC, only the Standard Model background processes, which are not affected by the choice of the MSSM parameters, will be taken into account.

4 Discovery potential for the neutral A and H Higgs bosons at CLIC

In order to estimate the discovery limits for AH pairs at CLIC, it is necessary to know the physics background first. A large number of processes may lead to hadronic final states. For many of them, the cross section is several orders of magnitude larger than for $e^+e^- \to AH$. However, the processes which have the largest cross sections, such as W boson or t quark pair production, lead only to four or six fermions, with two or less b quarks in the final state. Therefore, these backgrounds can be efficiently suppressed by a cut on the jet multiplicity and by requiring the presence of four b tagged jets. Furthermore, in the reconstruction algorithm of the $t\bar{t}t\bar{t}$ and $t\bar{t}b\bar{b}$ final states, the requirement on the masses of the intermediate states (i.e. the W bosons and the t quarks) reduces much further the event rates of the background processes in which the parton configuration differs from the signal.

The most significant background processes are those which lead to genuine $b\bar{b}b\bar{b}$, $t\bar{t}t\bar{t}$ or $t\bar{t}b\bar{b}$ final states. Their production cross section was calculated with the CompHEP event generator [12]. If neither ISR nor beamstrahlung is included, we find 0.96 fb for $e^+e^- \to b\bar{b}b\bar{b}$, 0.03 fb for $e^+e^- \to t\bar{t}t\bar{t}$ and 1.31 fb for $e^+e^- \to t\bar{t}b\bar{b}$. In CompHEP, it is possible to apply cuts on various phase space functions, while calculating the cross sections. Indeed, this prevents from producing background events which are not likely to contaminate the signal samples. A careful analysis of each background process was thus performed in order to determine whether it may seriously affect the signal reconstruction or not. In particular, the cross sections for $e^+e^- \to b\bar{b}b\bar{b}$, $e^+e^- \to t\bar{t}t\bar{t}$ and $e^+e^- \to t\bar{t}b\bar{b}$ were recalculated after having applied various cuts on the invariant mass of the quark-antiquark pairs, at the generator level.

In the case of $e^+e^- \to b\bar{b}b\bar{b}$ background events, the cross section becomes 0.031 fb (respectively 0.005 fb) if one requires that both $b\bar{b}$ pairs have an invariant mass larger than 500 GeV (respectively 1 TeV) at the generator level. This is much smaller than the cross section for $e^+e^- \to AH \to b\bar{b}b\bar{b}$. The event topology for the signal and for the background is indeed very different: in the first case, the $b\bar{b}$ pairs come from two heavy particles having exactly the same mass while, in the second case, the $b\bar{b}$ pairs usually come from a virtual γ/Z boson, a gluon or a Higgs boson (there is thus no reason why they should have the same invariant mass). As a result, at large values of m_A, the contribution of the $e^+e^- \to b\bar{b}b\bar{b}$ background remains negligible, especially if one also discards the reconstructed events for which the mass difference $\delta m = |m(bb)_1 - m(bb)_2|$ is too large. In the Standard Model, the $e^+e^- \to t\bar{t}t\bar{t}$ and $e^+e^- \to b\bar{b}b\bar{b}$ processes are very similar, and one can draw the same conclusion as previously: the contribution of the $e^+e^- \to t\bar{t}t\bar{t}$ background process remains negligible when reconstructing $e^+e^- \to AH \to t\bar{t}t\bar{t}$ events. Indeed, if one requires that both $t\bar{t}$ pairs have an invariant mass larger than 500 GeV (respectively 1 TeV) at the generator level, then the cross section for $e^+e^- \to t\bar{t}t\bar{t}$ is 0.019 fb (respectively 0.003 fb). Finally, a similar analysis was also performed for the $e^+e^- \to t\bar{t}b\bar{b}$ background. We noticed that, in most of the processes with $t\bar{t}b\bar{b}$ final states, t and $\bar{t}$, respectively b and $\bar{b}$, usually come from the same vertex. If one requires that the $b\bar{b}$ and $t\bar{t}$ pairs have an invariant mass larger than 500 GeV (respectively 1 TeV) at the generator level, then the cross section for $e^+e^- \to t\bar{t}b\bar{b}$ is 0.042 fb (respectively 0.010 fb). One can therefore also neglect the contribution of the $e^+e^- \to t\bar{t}b\bar{b}$ background at large m_A. For the sake of simplicity, these calculations were performed without ISR or beamstrahlung, but our conclusions are not significantly affected by them.

Having ensured a very good signal purity at large values of m_A, it is possible to derive the discovery limits for AH pairs at CLIC in terms of mass and branching ratios. For this purpose, we assume that the integrated luminosity is 3000 fb^{-1} and we require the number of signal events under the reconstructed mass peak to be at least 10 (the contribution of the Standard Model background is small enough to ensure that the significance remains larger than 5). For the large values of $tan\beta$, A and H mainly decay into $b\bar{b}$ pairs. When the corresponding branching ratio is maximal (i.e. 87%), the discovery limit is 1.39 TeV. For the small values of $tan\beta$, A and H essentially decay into $t\bar{t}$ pairs. When assuming that $\mathrm{Br}(A, H \to t\bar{t})$ is 100%, the discovery limit is 1.16 TeV. For the intermediate values of $tan\beta$, A and H can decay into $b\bar{b}$ and $t\bar{t}$ pairs. In addition to $e^+e^- \to AH \to b\bar{b}b\bar{b}$ and $e^+e^- \to AH \to t\bar{t}t\bar{t}$ events, one should also consider $t\bar{t}b\bar{b}$ final states. Their rate becomes maximal when $tan\beta \simeq 7$ and, in that case, $\mathrm{Br}(A, H \to t\bar{t}) = \mathrm{Br}(A, H \to b\bar{b}) \simeq 46.5\%$. The corresponding discovery limit is 0.96 TeV only, due to a smaller branching ratio than for the $b\bar{b}b\bar{b}$ and $t\bar{t}t\bar{t}$ final states. Note that we did not consider $e^+e^- \to H^+H^- \to t\bar{b}\bar{t}b$ events here, but the cuts reducing their contribution were used.

Various values of $tan\beta$ were considered in order to draw the whole discovery contour. For each of them, the branching ratios of the three possible final states were calculated. Knowing them, it is possible to derive the production cross section for AH pairs and thus the value of m_A leading to a discovery, for $b\bar{b}b\bar{b}$, $t\bar{t}t\bar{t}$ and $t\bar{t}b\bar{b}$ final states. The result of this study is shown in Figure 14.

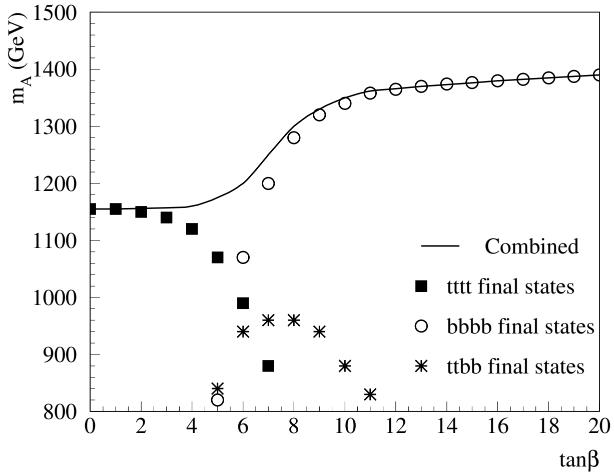

Figure 14: Discovery contour in the ($tan\beta$, m_A) plane for AH pairs at CLIC. The integrated luminosity is 3000 fb^{-1} and the hadronic background is taken into account with $N_{bc} = 15$.

These discovery limits were computed with a b tagging efficiency ϵ_b of 90% in the reconstruction procedure. This corresponds to a misidentification rate of 45% for c-jets while, for jets coming from u, d or s quarks, the misidentification rate is 20% [13]. When decreasing the b tagging efficiency and thus the non-b jet misidentification rate (for instance to better control the multi-jet background with less than four b quarks), the discovery limits become lower than in Figure 14. For the sake of simplicity, let us consider either small or large values of $tan\beta$, i.e. either $t\bar{t}t\bar{t}$ or $b\bar{b}b\bar{b}$ final states. In both cases, the contribution of the Standard Model background is small enough for the discovery limits to be essentially derived from the condition $S \geq 10$, where S is proportional to ϵ_b^4. Table 1 shows how the discovery limits at small and large $tan\beta$ vary with the b tagging efficiency (for information, the corresponding misidentification rates are also given).

b tagging efficiency	90%	80%	70%	60%
c-jet misidentification rate	45%	20%	10%	4%
uds-jet misidentification rate	20%	7%	0.5%	0.2%
Discovery limit at small $tan\beta$ (TeV)	1.16	1.07	0.97	0.81
Discovery limit at large $tan\beta$ (TeV)	1.39	1.34	1.28	1.20

Table 1: Variation with the b tagging efficiency of the non-b jet misidentification rates and of the discovery limit for AH pairs at small or large values of $tan\beta$.

5 Measurement of the neutral Higgs boson mass m_A and of the signal rate

In this section, we focus on the measurement of the mass of the neutral A and H Higgs bosons, as well as on the determination of the signal rate for $e^+e^- \rightarrow AH$, for the three possible final states. In the following, we will always consider an integrated luminosity of 3000 fb^{-1}.

5.1 Study of $b\bar{b}b\bar{b}$ final states

Let us first assume that the neutral Higgs bosons mainly decay into $b\bar{b}$ and that m_A is 876 GeV. In this case, the production cross section for AH pairs at CLIC was found to be 0.32 fb. Furthermore, if one chooses a large value of $tan\beta$, the branching ratio $\mathrm{Br}(A, H \rightarrow b\bar{b})$ is about 87%.

A sample of 720 "real" $e^+e^- \rightarrow AH \rightarrow b\bar{b}b\bar{b}$ events, which corresponds to a cross section $\sigma \cdot \mathrm{Br}^2$ of 0.24 fb, was generated, as well as various large samples of "simulated" $e^+e^- \rightarrow AH \rightarrow b\bar{b}b\bar{b}$ events, with different values for the mass and the cross section. Comparing the "real" and "simulated" samples then allows to derive the parameters of interest. Here, the hadronic background is taken into account ($N_{bc} = 15$) and the reconstruction procedure of Section 3.2 is used.

For each sample of "simulated" events, one calculates:

$$\chi^2 = \sum_i \frac{(N_r(i) - N_s(i))^2}{N_r(i)},$$

where $N_s(i)$ and $N_r(i)$ are respectively the number of "simulated" and "real" events in the bin i of the reconstructed mass histogram (here, the amount of "simulated" events is large enough to neglect the uncertainty on $N_s(i)$ in the estimation of χ^2). For Poisson-distributed data, minimizing χ^2 is equivalent to maximizing the likelihood function for the contents of the bins.

Let us choose several values of the cross section $\sigma \cdot \mathrm{Br}^2$ between 0.20 and 0.28 fb. For each of them, χ^2 is calculated as a function of the mass of the neutral Higgs bosons used in the "simulated" samples, and the minimal value of χ^2 is then derived from a parabolic fit. Knowing how $\mathrm{Min}(\chi^2)$ depends on the cross section, it is possible to derive the value of $\sigma \cdot \mathrm{Br}^2$ for which $\mathrm{Min}(\chi^2)$ is the smallest with a parabolic fit: we found $\sigma \cdot \mathrm{Br}^2 = 0.227 \pm 0.014$ fb. If this value is chosen for the cross section, then χ^2 becomes minimal when $m_A = 880.0 \pm 5.1$ GeV, see Figure 15. For this study, no mass constrained kinematical fit was used.

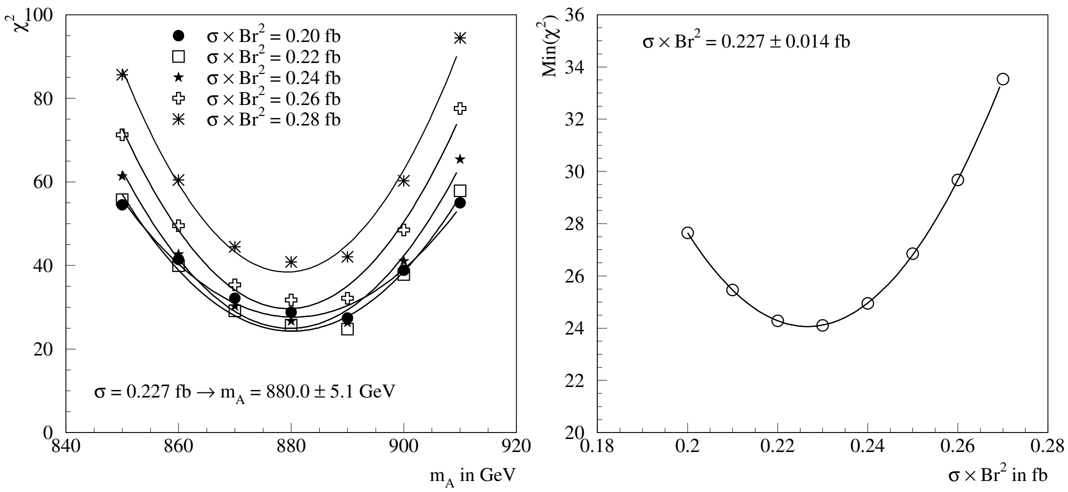

Figure 15: Determination of the statistical errors on m_A and on the cross section for $e^+e^- \to AH \to b\bar{b}b\bar{b}$. The variation of χ^2 with m_A is shown on the left, for various values of the cross section. The minimal value of χ^2 is derived from a parabolic fit. The variation of $\mathrm{Min}(\chi^2)$ with the cross section is shown on the right. Here, the integrated luminosity is 3000 fb^{-1} and $\mathrm{Br}(A, H \to b\bar{b}) = 87\%$.

A similar analysis was performed after using the kinematical fit. In that case, the minimisation of χ^2 leads to $\sigma \cdot \mathrm{Br}^2 = 0.246 \pm 0.015$ fb and $m_A = 873.0 \pm 3.7$ GeV. The measurement of m_A is therefore somewhat more accurate than without the kinematical fit, but the same conclusion can not be drawn for the signal rate.

Two other values of m_A were considered as well, and a similar analysis was performed to estimate the best relative accuracy for the determination of the mass and the signal rate. The results that we obtained are summarized in Table 2.

m_A in GeV	576	736	876
$\delta(\sigma \cdot \mathrm{Br}^2)/(\sigma \cdot \mathrm{Br}^2)$	3.3%	4.7%	6.2%
$\delta m/m$	0.4%	0.4%	0.4%

Table 2: Accuracy for the determination of the signal rate and of the neutral Higgs boson mass for different values of m_A, in the $e^+e^- \to AH \to b\bar{b}b\bar{b}$ channel: we consider an integrated luminosity of 3000 fb^{-1} and we assume that $tan\beta$ is large, i.e. $\mathrm{Br}(A, H \to b\bar{b}) = 87\%$.

5.2 Study of $t\bar{t}t\bar{t}$ final states

Let us assume that A and H only decay into $t\bar{t}$. A χ^2 analysis was performed for three different values of m_A: 576, 736 and 876 GeV. For each of them, a sample of "real" $e^+e^- \to AH \to t\bar{t}t\bar{t}$ events and various large samples of "simulated" events were generated and compared, after having used the reconstruction procedure of Section 3.3. The best relative accuracies that were obtained for the determination of the mass and the signal rate are reported in Table 3.

m_A in GeV	576	736	876
$\delta(\sigma \cdot \mathrm{Br}^2)/(\sigma \cdot \mathrm{Br}^2)$	7.5%	10.0%	15.3%
$\delta m/m$	1.2%	1.8%	2.7%

Table 3: Accuracy for the determination of the signal rate and of the neutral Higgs boson mass for different values of m_A, in the $e^+e^- \to AH \to t\bar{t}t\bar{t}$ channel: we consider an integrated luminosity of 3000 fb^{-1} and we assume that $tan\beta$ is small, i.e. $\mathrm{Br}(A, H \to t\bar{t}) = 100\%$.

Because of a smaller signal efficiency (due to a more complex event topology), the statistical errors obtained here are much larger than for $b\bar{b}b\bar{b}$ final states.

5.3 Study of $t\bar{t}b\bar{b}$ final states

For intermediate values of $tan\beta$, the production of AH pairs can lead to $t\bar{t}b\bar{b}$ final states. Let us assume that the corresponding signal rate is maximal, i.e. $tan\beta \simeq 7$. A χ^2 analysis was performed for three different values of m_A: 576, 736 and 876 GeV. The reconstruction procedure of Section 3.4 was used. The selection cuts which are used to reduce the contribution of the $e^+e^- \to H^+H^- \to t\bar{b}\bar{t}b$ events were applied but, for the sake of simplicity, these events themselves were not taken into account. The best relative accuracies that were obtained for the determination of the mass and the signal rate are reported in Table 4.

m_A in GeV	576	736	876
$\delta(\sigma \cdot \mathrm{Br}^2)/(\sigma \cdot \mathrm{Br}^2)$	10.2%	13.4%	20.2%
$\delta m/m$	1.6%	2.1%	2.7%

Table 4: Accuracy for the determination of the signal rate and of the neutral Higgs boson mass for different values of m_A, in the $e^+e^- \to AH \to t\bar{t}b\bar{b}$ channel: we consider an integrated luminosity of 3000 fb^{-1} and we assume that $tan\beta \simeq 7$, which corresponds to $\mathrm{Br}(A, H \to t\bar{t}) = \mathrm{Br}(A, H \to b\bar{b}) \simeq 46.5\%$

Because of a smaller branching ratio, the statistical errors obtained here are worse than for $b\bar{b}b\bar{b}$ and $t\bar{t}t\bar{t}$ final states (despite the fact that the signal efficiency is somewhat larger for $e^+e^- \to AH \to t\bar{t}b\bar{b}$ than for $e^+e^- \to AH \to t\bar{t}t\bar{t}$).

6 Determination of $tan\beta$

The ratio $tan\beta$ of the vacuum expectation values of the two Higgs doublets is a very important parameter in the MSSM. Various methods have been proposed in order to accurately measure it at linear e^+e^- colliders [14].

6.1 From the measurement of the signal rates

At first order, the total production cross section for AH pairs in e^+e^- collisions does not depend on the MSSM parameter $tan\beta$. It is indeed fully determined by m_A, $\sqrt{s}$ and the luminosity spectrum. Any uncertainty on the measured value of m_A thus induces errors when estimating the total production cross section σ for $e^+e^- \to AH$.

As for the branching ratios of A and H, they do vary with $tan\beta$, as it was shown in Figure 3. At large $tan\beta$, both A and H mainly decay into $b\bar{b}$ pairs and the branching ratio $\mathrm{Br}(A, H \to b\bar{b})$ remains constant: it is thus impossible to derive $tan\beta$ from the measured signal rate of $e^+e^- \to AH \to b\bar{b}b\bar{b}$. Instead, several values of $tan\beta$ were considered in the intermediate range, where A and H can decay into both $b\bar{b}$ and $t\bar{t}$ pairs. For each value of $tan\beta$, the branching ratios of A and H were estimated with HDECAY and the relative statistical error on the signal rate $\sigma \cdot \mathrm{Br}^2$ was derived from a χ^2-analysis, for each type of final state. The corresponding absolute uncertainty $\delta\mathrm{Br}$ on the "average" branching ratio was then estimated, taking into account the uncertainty in the determination of σ that is due to the statistical error on the measured value of m_A:

$$\mathrm{Br} = \sqrt{\frac{\sigma \cdot \mathrm{Br}^2}{\sigma}} \Longrightarrow \delta\mathrm{Br} = \frac{\mathrm{Br}}{2}\sqrt{\left(\frac{\delta(\sigma \cdot \mathrm{Br}^2)}{\sigma \cdot \mathrm{Br}^2}\right)^2 + \left(\frac{\delta\sigma}{\sigma}\right)^2},$$

where $\mathrm{Br} = \sqrt{\mathrm{Br}(A \to ...) \times \mathrm{Br}(H \to ...)}$ for each possible final state.

We noticed that the uncertainty on the "average" branching ratio mainly comes from the statistical error in the determination of the signal rate and to a lower extent on $\delta\sigma/\sigma$, thanks to an accurate measurement of m_A. However, we have not taken into account possible systematic errors on the energy and/or the luminosity spectrum, which may also affect the determination of the total production cross section σ.

Knowing how Br depends on $tan\beta$, one can then estimate the absolute error $\delta tan\beta$. The results obtained with this method are shown in Figures 16 to 18. The MSSM parameter $tan\beta$ is best measured where there is a fast variation of $\mathrm{Br}(A, H \rightarrow t\bar{t})$ and $\mathrm{Br}(A, H \rightarrow b\bar{b})$ with $tan\beta$.

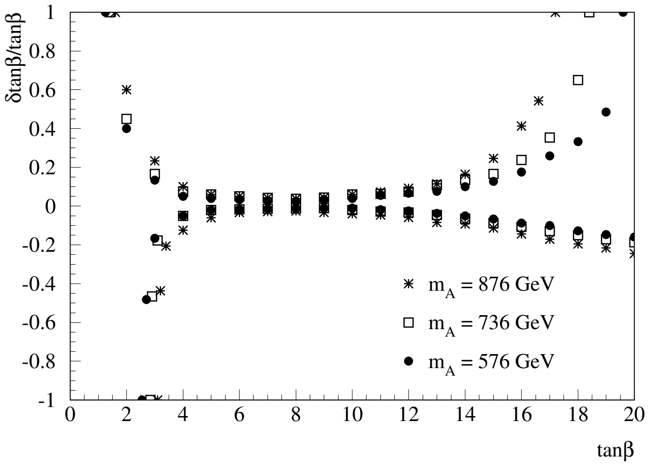

Figure 16: Relative statistical uncertainty in the determination of $tan\beta$ after having measured the signal rate of $e^+e^- \rightarrow AH \rightarrow b\bar{b}b\bar{b}$. These calculations were performed for three different values of m_A.

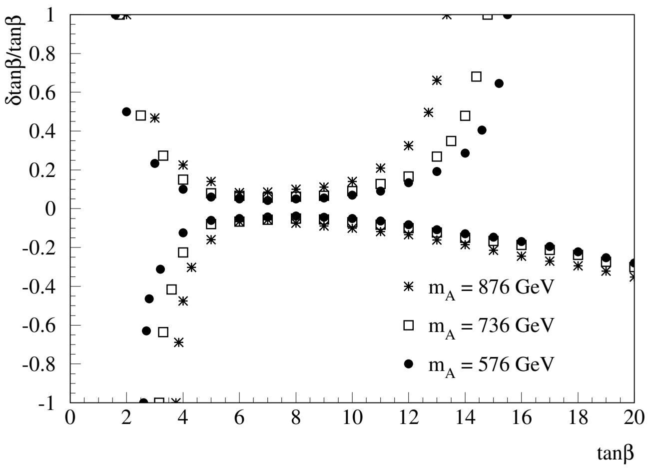

Figure 17: Relative statistical uncertainty in the determination of $tan\beta$ after having measured the signal rate of $e^+e^- \rightarrow AH \rightarrow t\bar{t}t\bar{t}$. These calculations were performed for three different values of m_A.

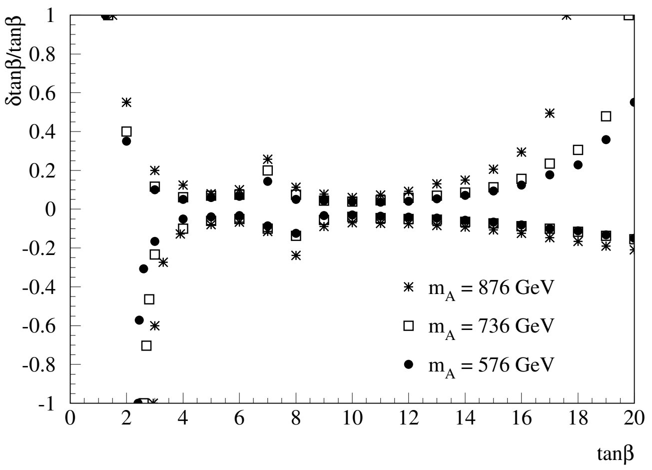

Figure 18: Relative statistical uncertainty in the determination of $tan\beta$ after having measured the signal rate of $e^+e^- \to AH \to t\bar{t}b\bar{b}$. These calculations were performed for three different values of m_A.

In the case of $e^+e^- \to AH \to t\bar{t}b\bar{b}$, note that one value of the "average" branching ratio Br may correspond to two different values of $tan\beta$, as illustrated in Figure 4. In general, one can distinguish between the two possible values of $tan\beta$ by also using the information which is contained in the signal rate for $e^+e^- \to AH \to b\bar{b}b\bar{b}$ and $e^+e^- \to AH \to t\bar{t}t\bar{t}$, except when Br is close to its maximum value, which corresponds to $tan\beta \simeq 7$.

6.2 From the ratio $\mathrm{Br}(A,H \to b\bar{b})\,/\,\mathrm{Br}(A,H \to t\bar{t})$

The determination of $tan\beta$ from the measured signal rate $\sigma \cdot \mathrm{Br}^2$ has one major drawback: one can not easily derive the total production cross-section from only m_A, the centre-of-mass energy and the luminosity spectrum, because high-order effects should be also taken into account. As a result, σ should be considered as an unknown parameter, which makes the determination of $tan\beta$ through the measurement of the signal rates much more difficult.

Let us define the ratio $r = \sqrt{\dfrac{\mathrm{Br}(H \to b\bar{b}) \cdot \mathrm{Br}(A \to b\bar{b})}{\mathrm{Br}(H \to t\bar{t}) \cdot \mathrm{Br}(A \to t\bar{t})}}$.

The error on r can be written as $\delta r = \dfrac{r}{2}\sqrt{\left(\dfrac{\delta(\sigma \cdot \mathrm{Br}^2)}{\sigma \cdot \mathrm{Br}^2}\right)^2_{b\bar{b}b\bar{b}} + \left(\dfrac{\delta(\sigma \cdot \mathrm{Br}^2)}{\sigma \cdot \mathrm{Br}^2}\right)^2_{t\bar{t}t\bar{t}}}$.

The error δr only depends on the relative statistical uncertainties on the signal rates for $b\bar{b}b\bar{b}$ or $t\bar{t}t\bar{t}$ final states. Knowing how the ratio r depends on $tan\beta$ (as illustrated in the left-hand side plot of Figure 19) and knowing the statistical accuracies for the signal rate of $e^+e^- \to AH \to b\bar{b}b\bar{b}$ and $e^+e^- \to AH \to t\bar{t}t\bar{t}$ events for various values of $tan\beta$, one can estimate the absolute error $\delta tan\beta$.

The results obtained with this method are shown in the right-hand side plot of Figure 19: the MSSM parameter $tan\beta$ can be determined with a relative error of less than 20% (respectively 10%) in the 3-13 (respectively 4-10) range.

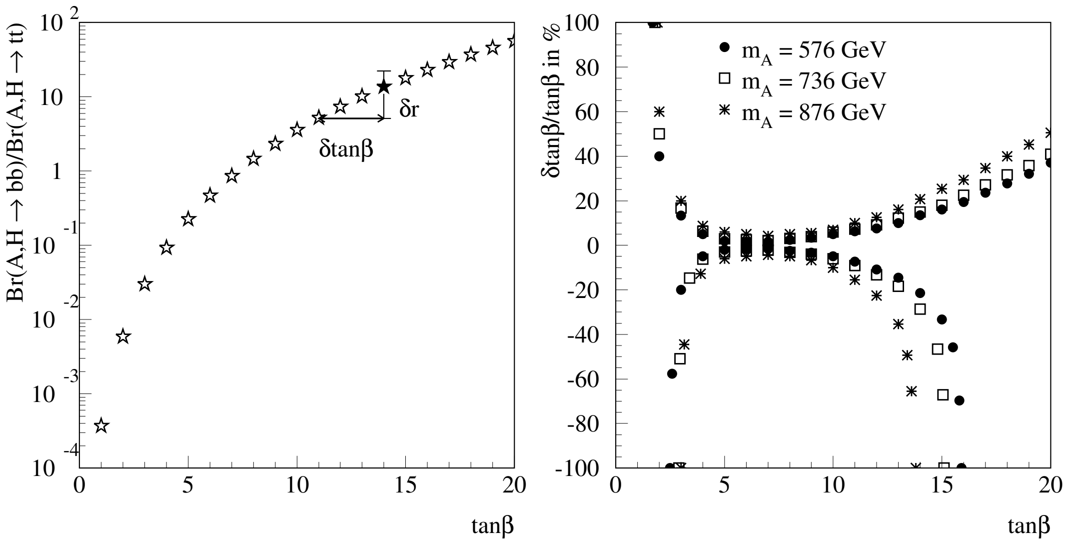

Figure 19: Estimation of the relative statistical uncertainty in the determination of $tan\beta$ through the measurement of the ratio r between Br$(A, H \to b\bar{b})$ and Br$(A, H \to t\bar{t})$, for various values of m_A.

6.3 From the measurement of the width

The MSSM parameter $tan\beta$ controls the partial widths of the neutral A and H Higgs bosons. However, calculations with HDECAY show that their natural width is always much smaller than the experimental mass resolution, as it is shown in Table 5. An accurate measurement of Γ_A or Γ_H and the subsequent determination of $tan\beta$ are therefore extremely difficult.

m_A in GeV $tan\beta$	576 2/10/20	736 2/10/20	876 2/10/20
$\Gamma(A/H \to b\bar{b})$ in GeV	-/1.0/4.3	-/1.3/5.4	-/1.6/6.2
Experimental fwhm in GeV	56.9	47.7	45.8
$\Gamma(A/H \to t\bar{t})$ in GeV	6.0/0.3/-	9.1/0.4/-	11.8/0.5/-
Experimental fwhm in GeV	124.1	121.0	133.9

Table 5: Comparison of the partial widths for some hadronic decays of the A and H Higgs bosons with the experimental mass resolution (fwhm = full width at half of the maximum amplitude), as obtained after having forced $\Gamma(A, H)$ to be zero in PYTHIA. Note that the natural partial widths are obtained by taking the average of $\Gamma(A \to ...)$ and $\Gamma(H \to ...)$, for the sake of simplicity.

7 Conclusion

In this paper, we have studied the production of AH pairs in e^+e^- collisions at $\sqrt{s} = 3$ TeV. Only the decays into third generation quarks ($A, H \to b\bar{b}$ and $A, H \to t\bar{t}$) were considered here, because they have a larger branching ratio than $A, H \to \tau^+\tau^-$ and other decay modes. The final states of interest thus consist of four b quarks, either alone or accompanied by two or four W bosons, depending on the decay chain that one considers (the production of AH pairs may indeed lead to $b\bar{b}b\bar{b}$, $t\bar{t}b\bar{b}$ or $t\bar{t}t\bar{t}$ final states). Only the hadronic decays of the W bosons were studied here, which lead to highly distinctive, yet challenging, multi-jet final states with four b tagged jets. In the reconstruction procedures, special care was taken in order to make our results robust in the presence of CLIC high energy beam-beam effects, in particular beamstrahlung and additional $\gamma\gamma \to$ hadrons events.

With an integrated luminosity of 3000 fb^{-1} and a b tagging efficiency of 90%, AH pairs can be discovered at CLIC if m_A remains smaller than 1.2 TeV at low $tan\beta$, i.e. when the $t\bar{t}t\bar{t}$ final states are dominant, or 1.4 TeV at large $tan\beta$, i.e. when the $b\bar{b}b\bar{b}$ final states are dominant. Lower discovery limits are obtained with a decreased b tagging efficiency. The Higgs boson mass m_A and the signal rates of the various decay chains were measured with a χ^2-analysis. A very good accuracy was obtained for m_A as the statistical error is only a few percent. From the measurement and the comparison of the signal rates for $e^+e^- \to AH \to b\bar{b}b\bar{b}$ and $e^+e^- \to AH \to t\bar{t}t\bar{t}$, we showed that it was possible to determine $tan\beta$ in the 4-10 range with an accuracy better than 10%. Note that this region is not accessible through the study of charged Higgs bosons in pp collisions at LHC.

For a complete study of the neutral A and H Higgs bosons at CLIC, one should take more carefully into account the contribution of $e^+e^- \rightarrow H^+H^- \rightarrow t\bar{b}\bar{t}b$ events. In some cases, they may mimic the production of an AH pair. In this study, we have always neglected these events, however their influence could be investigated in more detail. For completeness, one should also take into account the decay of A and H into supersymmetric particles. They may provide additional information on the Higgs sector of the MSSM. They are also likely to have an influence on the branching ratios of the standard decays of A and H, which may then depend not only on $tan\beta$ but also on other MSSM parameters.

Acknowledgements

The author wishes to thank A. Sherstnev for his explanations regarding the use of CompHEP, as well as M. Battaglia, A. Djouadi and A. de Roeck for fruitful discussions and helpful advices.

References

[1] CLIC study team, *A 3 TeV e^+e^- linear collider based on CLIC technology*, CERN 2000-008.

[2] A. Ferrari, *Pair production of charged Higgs bosons in e+e- collisions at CLIC*, LC note LC-PHSM-2003-051.

[3] P. Janot, *Higgs boson searches at a 500 GeV e+e- collider*, proceedings of "Physics and Experiments with e+e- Linear Colliders", Waikoloa, Hawaii, 1993, ed. F. Harris, S. Olsen, S. Pakvasa and X. Tata, World Scientific 1993.

[4] A. Andreazza and C. Troncon, *Study of HA production in e+e- collisions at $\sqrt{s}$ = 800 GeV*, DESY 97-123E (417-428).

[5] G. Gamberini, J.F. Gunion, H.E. Habber, B. Kayser, S.F. Novaes, F. Olness, L. Roszkowski, A. Turski and J. Wudka, *Production mechanisms for non-minimal Higgs bosons at an e+e- collider*, Phys. Rev. D38 (1988) 3444.

[6] D. Schulte, *Background at future linear colliders*, CERN-PS-99-066.

[7] D. Schulte, *High energy beam-beam effects in CLIC*, CERN-PS-99-017 (LP).

[8] T. Sjöstrand, Comp. Phys. Comm. 82 (1994) 74.

[9] A. Djouadi, J. Kalinowski and P.M. Zerwas, *Two- and three-body decay modes of SUSY Higgs particles*, Z. Phys. C70 (1996) 435.

[10] A. Djouadi, J. Kalinowski and M. Spira, *HDECAY: a program for Higgs boson decays in the Standard Model and its Supersymmetric extension*, Comp. Phys. Comm. 108 (1998) 56.

[11] M. Pohl and H.J. Schreiber, *SIMDET - Version 3, a parametric Monte Carlo for a TESLA detector*, DESY 99-030.

[12] A. Pukhov, E. Boos, M. Dubinin, V. Edneral, V. Ilyin, D. Kovalenko, A. Kryukov, V. Savrin, S. Shichanin and A. Semenov, *CompHEP - a package for evaluation of Feynman diagrams and integration over multi-particle phase space, User's manual for version 33*, hep-ph/9908288.

[13] M. Battaglia, private communications.

[14] J. Gunion, T. Han, J. Jiang, and A. Sopczak, *Determining tanβ with neutral and charged Higgs bosons*, LC note LC-PHSM-2003-064.